# No evidence for entrainment: endogenous gamma oscillations and rhythmic flicker responses coexist in visual cortex

Katharina Duecker[1]*, Tjerk P. Gutteling[1], Christoph S. Herrmann[2], and Ole Jensen[1]*

[1]: University of Birmingham, School of Psychology, Centre for Human Brain Health, Birmingham, UK

[2]: Carl-von-Ossietzky University of Oldenburg, Faculty VI - Medicine and Health Sciences, Department of Psychology, Oldenburg, Germany

**Correspondence:** kxd888@student.bham.ac.uk, o.jensen@bham.ac.uk

## Abstract

Motivated by the plethora of studies associating gamma oscillations (∼30-100 Hz) with various neuronal processes, including inter-regional communication and neuroprotection, we asked if endogenous gamma oscillations in the human brain can be entrained by rhythmic photic stimulation. The photic drive produced a robust Magnetoencephalography (MEG) response in visual cortex up to frequencies of about 80 Hz. Strong, endogenous gamma oscillations were induced using moving grating stimuli as repeatedly shown in previous research. When superimposing the flicker and the gratings, there was no evidence for phase or frequency entrainment of the endogenous gamma oscillations by the photic drive. Rather – as supported by source modelling – our results show that the flicker response and the endogenous gamma oscillations coexist and are generated by different neuronal populations in visual cortex. Our findings challenge the notion that neuronal entrainment by visual stimulation generalises to cortical gamma oscillations.

**Key words:** Magnetoencephalography; Neuronal Oscillations; Entrainment; Gamma Oscillations; Frequency Tagging; Flicker; Photic drive

## Introduction

Neuronal cell assemblies have long been known to synchronise their discharges with millisecond precision (Buzsáki et al., 1992; Traub et al., 1996; Singer, 1999; Varela et al., 2001). This synchronisation has been linked to oscillatory activity in the gamma-frequency band (∼30-100 Hz) in various brain regions and species, e.g in rodents and primates (e.g. Eckhorn et al., 1988; Gray & Singer, 1989; Engel et al., 1992; Wehr & Laurent, 1996; Brosch et al., 2002), including humans (e.g. Tallon et al., 1995; Müller et al., 1997; Rodriguez et al., 1999; Hoogenboom et al., 2006). Neuronal gamma oscillations have been proposed to support neuronal computations within populations (Singer & Gray, 1995; Singer, 1999; Von der Malsburg, 1999; Engel et al., 2001; Singer, 2009; Nikolić et al., 2013) as well as inter-regional functional connectivity through coherence (Bressler, 1990; Varela et al., 2001; Fries et al., 2007). Furthermore, they have been associated with various cognitive functions (see Başar-Eroglu et al., 1996; Herrmann & Mecklinger, 2001; Jensen et al., 2007; Tallon-Baudry, 2009; Uhlhaas et al., 2009, for review). In accordance with that, anomalies in gamma-band activity have been reported in neurological and psychological disorders that are related to impaired cognition and awareness, such as Autism Spectrum Disorder, Schizophrenia and Alzheimer's Dementia (see Herrmann & Demiralp, 2005; Uhlhaas & Singer, 2006; Uhlhaas et al., 2009; Traub & Whittington, 2010; Grützner et al., 2013, for review). In this study, we aimed to investigate if endogenous gamma oscillations in the human visual system can be driven non-invasively by rhythmic photic stimulation. Developing a methodology to directly manipulate gamma oscillations would allow to probe their role in neuronal processing and cognition, as well as their therapeutic potential. Indeed, in rodents, oscillatory neuronal responses to both optogenetics and a visual flicker at 40 Hz have been associated with neuroprotective responses and reduced neuroinflammation (Iaccarino et al., 2016; Adaikkan et al., 2019); making it a promising tool to reverse neurodegeneration linked to Alzheimer's Dementia. These findings have been explained by an *entrainment*. i.e. a synchronisation, of intrinsic gamma oscillations with the stimulation (Adaikkan & Tsai, 2020). The prerequisite of entrainment, as considered in dynamical systems theory, is the presence of a self-sustained oscillator that synchronises to the external drive (Pikovsky et al., 2003). This definition has often not been sufficiently embraced in studies of neuronal entrainment to sensory stimulation, as pointed out by Helfrich et al. (2019). A related phenomenon that is reflected by periodic responses to a rhythmic drive and an amplification of individually preferred rhythms is *resonance*

2

51 (Hutcheon & Yarom, 2000). Resonance does however not require the presence of self-sustained oscillations

52 per se (Pikovsky et al., 2003; Helfrich et al., 2019). Indeed, oscillatory activity in response to a photic drive

53 at frequencies ranging from 1 to up to 100 Hz in human Electroencephalography (EEG) recordings, have

54 revealed a selective amplification of frequencies in the gamma band (Herrmann, 2001; Gulbinaite et al.,

55 2019), indicating resonance in the visual cortex. Here, we explore both resonance and entrainment in the

56 visual system to a visual flicker at frequencies >50 Hz. Stimulation at such high frequencies has recently

57 been applied in Rapid Frequency Tagging (RFT) protocols, to investigate spatial attention (Zhigalov et al.,

58 2019) and audiovisual integration in speech (Drijvers et al., 2020, bioRxiv), with minimal visibility of the

59 flicker.

60     Oscillatory responses to photic stimulation from 52 to 90 Hz, recorded with MEG, were investigated in

61 the presence and absence of visually induced gamma oscillations. In the *flicker* condition, the rhythmic drive

62 was applied to a circular, invisible patch. In the *flicker&gratings* condition, the flicker was superimposed

63 on moving grating stimuli that have been shown to reliably induce gamma oscillations (Hoogenboom et

64 al., 2006, 2010; Van Pelt & Fries, 2013), thus meeting the precondition for entrainment. We expected the

65 resonance properties of the visual system to change in presence of the endogenous gamma oscillations,

66 as well as a synchronisation of the endogenous gamma oscillations with the rhythmic flicker. As we will

67 demonstrate, the moving gratings did generate strong endogenous gamma oscillations, and the photic drive

68 did produce robust responses at frequencies up to 80 Hz. However, to our great surprise, there was no

69 evidence that the rhythmic stimulation entrains endogenous gamma oscillations.

## Results

71 The aim of the current study was to characterise entrainment and resonance properties in the visual cortex

72 in absence and presence of gamma-band oscillations induced by visual gratings. To this end, we drove

73 the visual cortex with a rapid flicker at frequencies ranging from 52 to 90 Hz, in steps of 2 Hz. The photic

74 drive was applied either to a circular patch (the *flicker* condition, Figure 10A,C) or to the light grey rings of a

75 moving grating stimulus (the *flicker&gratings* condition, Figure 10B,D). We hypothesised that a photic drive

76 within the frequency range close to the individual gamma frequency in the *flicker&gratings* condition would

77 entrain the grating-induced oscillations. This would be observed as the endogenous gamma oscillation

78  synchronising with the drive. Moreover, we expected the presence of the induced gamma oscillator to change

79  the resonance properties (compared to the *flicker* condition), reflected by an amplification of responses to

80  stimulation frequencies equal or close to the endogenous gamma rhythm. Response magnitudes in the

81  *flicker* condition were expected to reveal resonance properties of the visual system in absence of gamma

82  oscillations, demonstrating favourable stimulation frequencies to be used in future experiments applying

83  Rapid Frequency Tagging (RFT; Zhigalov et al., 2019; Drijvers et al., 2020).

## Identifying Individual Gamma Frequencies

85  The frequency of the endogenous gamma rhythm is known to vary between participants (Hoogenboom et

86  al., 2006, 2010; Muthukumaraswamy et al., 2010). Therefore, each subject's Individual Gamma Frequency

87  (IGF) was identified first, based on the 0 - 2 s interval in the *flicker&gratings* condition during which

88  the moving grating stimuli were presented without the visual flicker (Figure 10C). The Time-Frequency

89  Representations (TFRs) of power are depicted in Figure 1A,B for two representative participants. The centre

90  column shows the power averaged over time (0.25 - 1.75 s after the stimulus onset to avoid any event-related

91  field confounds) demonstrating distinct peaks at 58 and 74 Hz for these participants. The topographies in the

92  right column depict relative power change at the identified frequencies, focally in sensors over the occipital

93  cortex. For each subject, the 2 - 3 combined planar gradiometers showing maximum relative power change

94  in the gamma band were selected for further analysis (Sensors-of-Interest; SOI) per visual inspection. These

95  sensors strongly overlapped between participants. The data of participants with an IGF closer than 6 Hz to

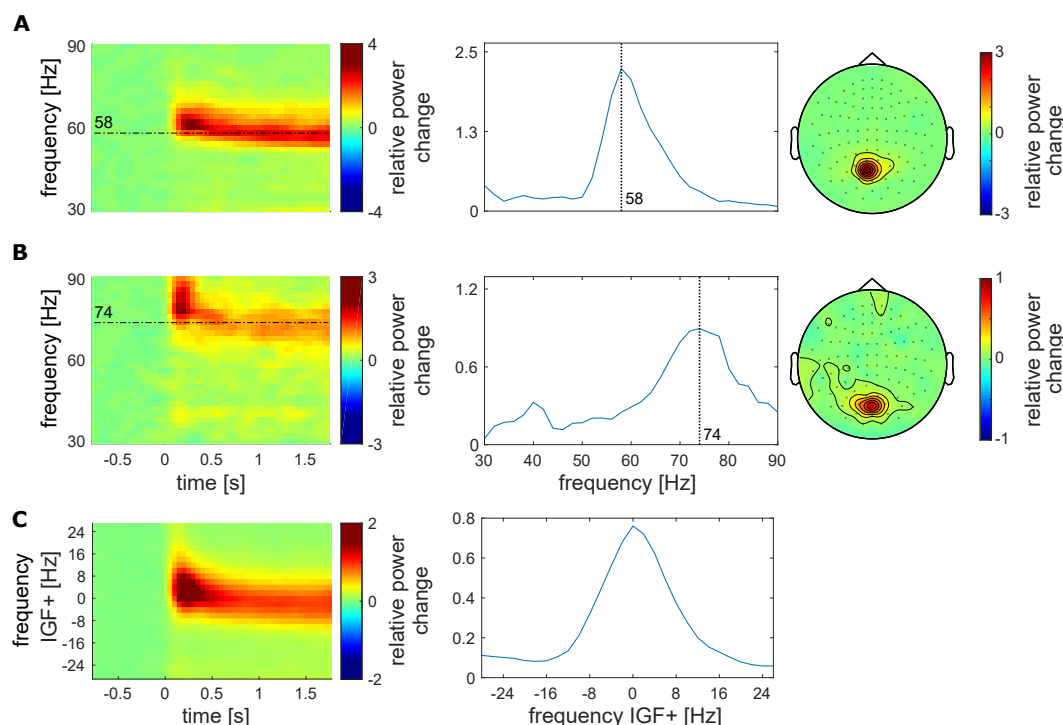96  the lowest (52 Hz) drive, i.e. IGF<58 Hz, were not considered for further analyses.

Figure 1: Identification of Individual Gamma Frequencies (IGF) and Sensors-of-Interest (SOI). **A, B** The TFRs of power, power spectra (averaged over 0.25 - 1.75 s) and topographic representations (combined planar gradiometers) of the IGF for two representative participants. The TFRs of power were calculated from the Fourier Transforms using a 500 ms sliding window, resulting in spectral smoothing of $\pm 3$ Hz. The IGFs were identified from the spectral peak in 0.25 - 1.75s interval of the TFRs. Identified IGFs are indicated by dashed lines. **C** The grand-average of the power analysis after aligning the individual TFRs and spectra to the IGF (N=22).

97  Figure 1C depicts the averaged TFRs of power as well as the power spectrum for the remaining subjects

98  (N=22), aligned to each participant's IGF prior to averaging. The moving grating stimulus induced sus-

99  tained oscillatory activity constrained to the IGF $\pm$ 8 Hz, with an average relative power change of 80% in

100  the 0.25 - 1.75 s interval compared to baseline. In short, the moving gratings produced robust gamma oscil-

101  lations observable in the individual participants which reliably allowed us to identify the individual gamma

102  frequencies.

## Photic drive induces responses up to ∼80 Hz

We next set out to quantify the rhythmic response to the flicker as a function of frequency in the *flicker* condition, in which stimulation was applied to an invisible patch. Figure 2 A and B, left panel, depicts the overlaid power spectra for the different stimulation frequencies in two representative participants (the same as in Figure 1). The spectra were estimated by averaging the TFRs of power in the 0.25 - 1.75s interval after flicker onset. Due to the overlap of the sensors detecting the gamma oscillations and photic drive response (compare Figure 1 and 2 right columns) the same SOI were used as in the *flicker&gratings* condition. Both individuals showed strong responses at the respective stimulation frequencies, with a maximum relative power change of 200% and 500% in subject A and B, respectively. It should be noted that the IGFs (indicated by vertical dashed lines) did not relate to the frequencies where the strongest RFT signal occurred (r(21) = 0.038, p = 0.87, *flicker* condition). When averaged over all participants, the magnitude of the flicker response decreased systematically with frequency (Figure 2**C**).
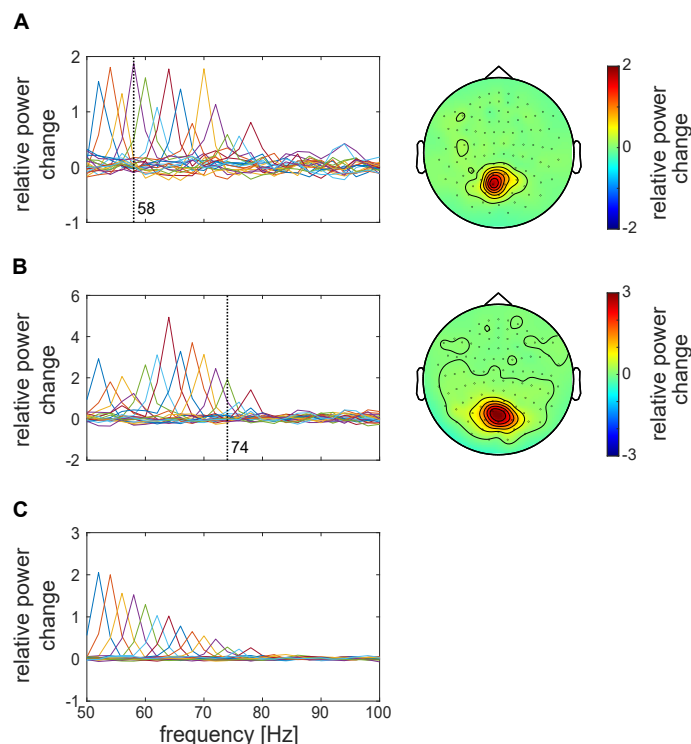
Figure 2: **A,B** The response to the photic drive in the *flicker* condition and the corresponding topographies for two representative subjects. Spectra were estimated from the TFRs of power averaged in the 0.25 - 1.75 s interval. Dashed vertical lines indicate the participants' IGF. The topographies (combined planar gradiometers) demonstrate a strong overlap with the ones in Figure 1. **C** Grand-average of the responses to the photic drive for each flicker frequency. On average, the magnitude of the flicker response decreases with increasing frequency, and is identifiable for stimulation below 80 Hz.

Figure 3A displays the power spectra in the *flicker* condition, estimated from the TFRs as explained above, averaged over all participants, as a function of stimulation frequency. These are equivalent to 2C. Diagonal values indicate the magnitude of the oscillatory responses (relative to baseline) at the stimulation frequencies, reaching values of up to 300% and decreasing monotonically with frequency. This confirms an upper limit for the stimulation of around 80 Hz. Off-diagonal values indicate oscillatory activity at frequencies different from the stimulation frequency. Figure 3B shows the same spectra after aligning to the individual IGFs, prior to averaging. Figure 3C and D display the spectra in the *flicker&gratings* condition

122 (averaged in the 2.25 - 3.75s interval), during which the photic drive was applied to the moving grating

123 stimulus (see Figure 10B). The induced gamma band activity can be observed as the horizontal yellow band

124 at ∼60 Hz. When aligning the spectra to the IGF (Figure 3D), we observe a decrease in the flicker response

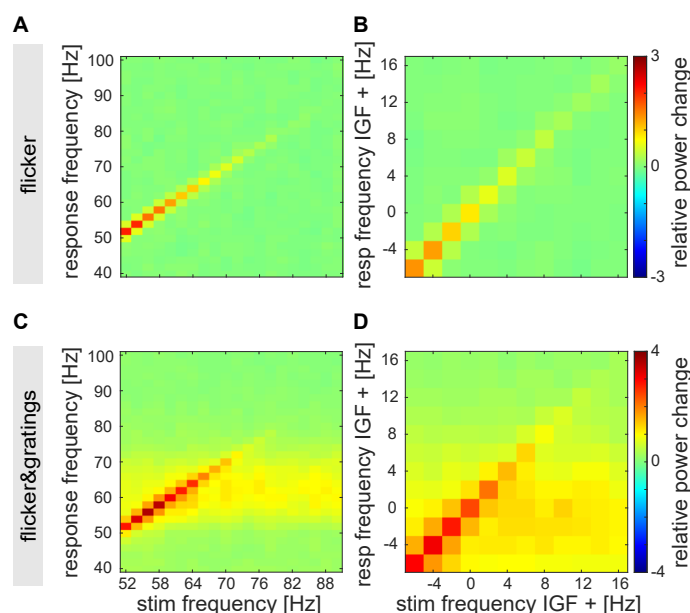125 but no evidence for an amplification at or close to the IGF.



Figure 3: Average relative power change to the photic drive (y-axis) with respect to the driving frequencies (x-axis) **A** The *flicker* condition. Note that the power changes mirror Figure 2**C**. Power decreases with increasing frequency, from a relative change of ∼3 at 52 HZ to ∼.5 at 80 Hz. **B** The *flicker* condition after the spectra were aligned to the IGF. **C** The *flicker&gratings* condition. All spectra demonstrate both the flicker response and induced gamma oscillation (observed as the yellow/orange horizontal band). Again, the amplitude of the rhythmic stimulation response appears to decrease with increasing frequency in both conditions. **D** The spectra for the *flicker&gratings* condition now aligned to the IGF. There is no indication that the rhythmic flicker captures the endogenous gamma oscillations.

## Magnitude of flicker response decreases as a function of frequency

127 The averaged TFRs of power in Figure 3 point to an approximately linear decrease in power of the flicker

128 response with increasing frequency. Literature on neural resonance and entrainment, however, suggests the

8

129  existence of a preferred rhythm at which oscillatory responses are amplified (Hutcheon & Yarom, 2000; Her-

130  rmann, 2001; Pikovsky et al., 2003; Notbohm et al., 2016; Gulbinaite et al., 2019). As argued in Pikovsky et

131  al. (2003) phase-locking between the driving signal and the self-sustained oscillator is the most appropriate

132  metric to investigate entrainment. Figure 4A,B depicts the phase-locking value (PLV) between the photodi-

133  ode and the MEG signal at the SOI (planar gradiometers, not combined). This measure reveals a systematic

134  decrease in phase-locking with increasing flicker frequency for both the *flicker* (orange) and *flicker&gratings*

135  (blue) condition (A). The observed relationship is preserved when aligning the frequencies to the IGF (B,

136  also see Table 1). Note the absence of increased phase-locking at the IGF. The magnitude of the flicker

137  response, quantified by power change compared to baseline, as a function of frequency, is demonstrated in

138  Figure 4C-F and depicts a similar relationship to the one observed for the PLV. The *flicker* condition (C, or-

139  ange line) revealed a systematic decrease with frequency, whereas the *flicker&gratings* condition did show

140  a peak at 56 Hz. However, this observed increase appeared to be caused by considerable variance between

141  the power estimates of the individual participants (see Figure 4E, each line graph depicts power estimates

142  per individual participant). We again aligned the spectra to the IGF before computing the grand-average

143  (Figure 4D). The absence of a peak at 0 Hz suggests no evidence for resonance at the IGF, confirming the

144  peak at 56 Hz in C to be the result of inter-subject variability. Indeed, simple linear regression models, fit

145  individually to PLV and power as a function of frequency aligned to the IGF, separately for each condition,

146  explain a considerable amount of the variance (see Table 1 and dotted lines in Figure 4). We then identified

147  the individual peak frequencies, eliciting the strongest response to the flicker in the *flicker&gratings* condi-

148  tion 4E, and related those to the IGF, as seen in Figure 4F. Importantly, the frequency inducing the strongest

149  response to the rhythmic drive was below the IGF in the majority of participants, whereby the frequencies

150  turned out to be uncorrelated (r(21)=-0.15, p =0.5, *flicker&gratings* condition).
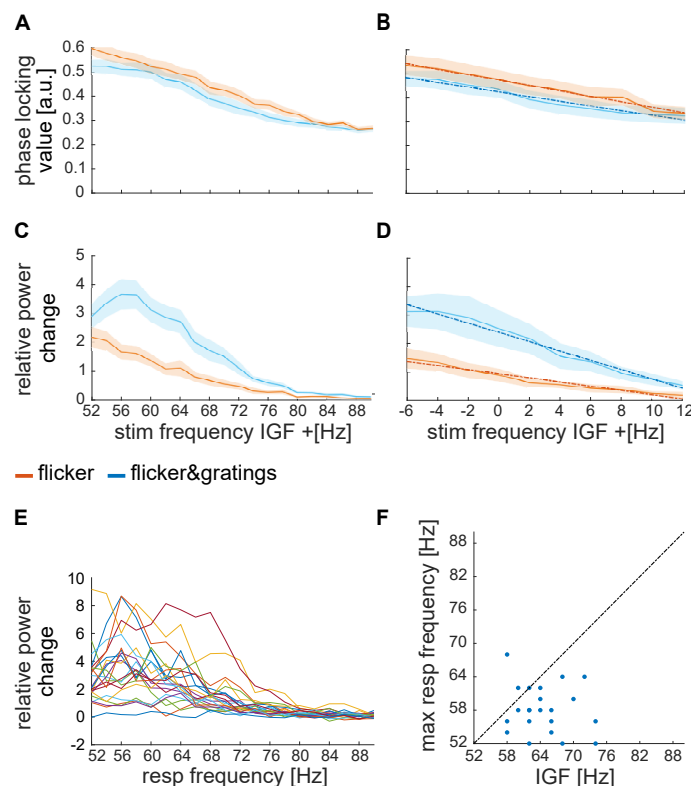
9

Figure 4: Magnitude of the flicker response as a function of frequency in the *flicker* (orange) and *flicker&gratings* (blue) condition. **A** The phase-locking values between the photo-diode and the MEG signal over the SOIs as a function of driving frequency. **B** The phase-locking values between the photo-diode and the MEG signals as a function of frequency after the spectra were aligned to IGF. Again, the phase-locking decreases with increasing frequency (see Table 1 for a statistical quantification of the simple linear regression models). **C** Relative power change with respect to baseline as a function of frequency. Generally, the power decreased with frequency, however, in the *flicker&gratings* there is an apparent peak at ∼56 Hz; yet, the shaded errors (SE) indicate considerable variance between participants. **D** The relative power spectra as a function of frequency after the individual spectra were aligned in frequency according to the IGF, demonstrating that responses to a photic drive at the IGF are not amplified. **E** Relative power change as a function of frequency for each individual subject (N = 22), indicates that the peak at ∼56 Hz in **C** is driven by comparably high power in that frequency range in just a few individuals. **F** Flicker frequency inducing highest power values versus IGF, demonstrating no systematic relationship ($r(21) = -0.15, p = .5$). Instead, the frequencies inducing maximum power change were below the IGF in the majority of participants.

10

Table 1: Simple linear regression models: Flicker response magnitude as a function of distance to IGF.

| Model | Estimates | | | | |
|---|---|---|---|---|---|
| | $\beta_1$ | t | p *** | $R^2$ | F(1,218) |
| *flicker $_{plv}$* | $-.01$ | $-8.07$ | $< 2.2e - 16$ | .23 | 65.07 |
| *flicker&gratings $_{plv}$* | $-.01$ | $-7.24$ | $< 2.2e - 16$ | .19 | 52.44 |
| *flicker $_{pow}$* | $-.07$ | $-9.01$ | $4.80e - 14$ | .27 | 81.14 |
| *flicker&gratings $_{pow}$* | $-.16$ | $-8.95$ | $7.51e - 12$ | .27 | 80.13 |

## Gamma oscillations and flicker response coexist

We initially hypothesised that entrainment of the gamma oscillations in the *flicker&gratings* condition would result in the photic drive capturing the oscillatory dynamics when the driving frequency was close to endogenous gamma oscillations. Figure 5 depicts the TFRs of power relative to a 0.5 s baseline, for one representative subject (also shown in Figure 1 and 2A). The averaged trials for a photic drive at 52 Hz are shown in Figure 5A and separately for each flicker frequency in Figure 5B (Figure created using Kumpulainen, n.d.). The IGF (58 Hz for this subject) and the respective stimulation frequencies are indicated by dashed lines. The endogenous gamma oscillations, induced by the moving grating stimulus, are observed as the sustained power increase from 0 - 6 s whereas the flicker response is demonstrated by a power increase at 2 - 4 s. The plots reveal that gamma oscillations persist at the IGF and coexist with the response to the photic drive, which is particularly apparent for stimulation at 52 Hz (Figure 5 A). Furthermore, the power increase at the flicker frequency does not appear to outlast termination of the drive at t = 4 s. In the subsequent step, we frequency-aligned the TFRs of power according to the IGF before averaging over participants. Again, the analyses were constrained to individuals with an IGF above 56 Hz (N = 22).
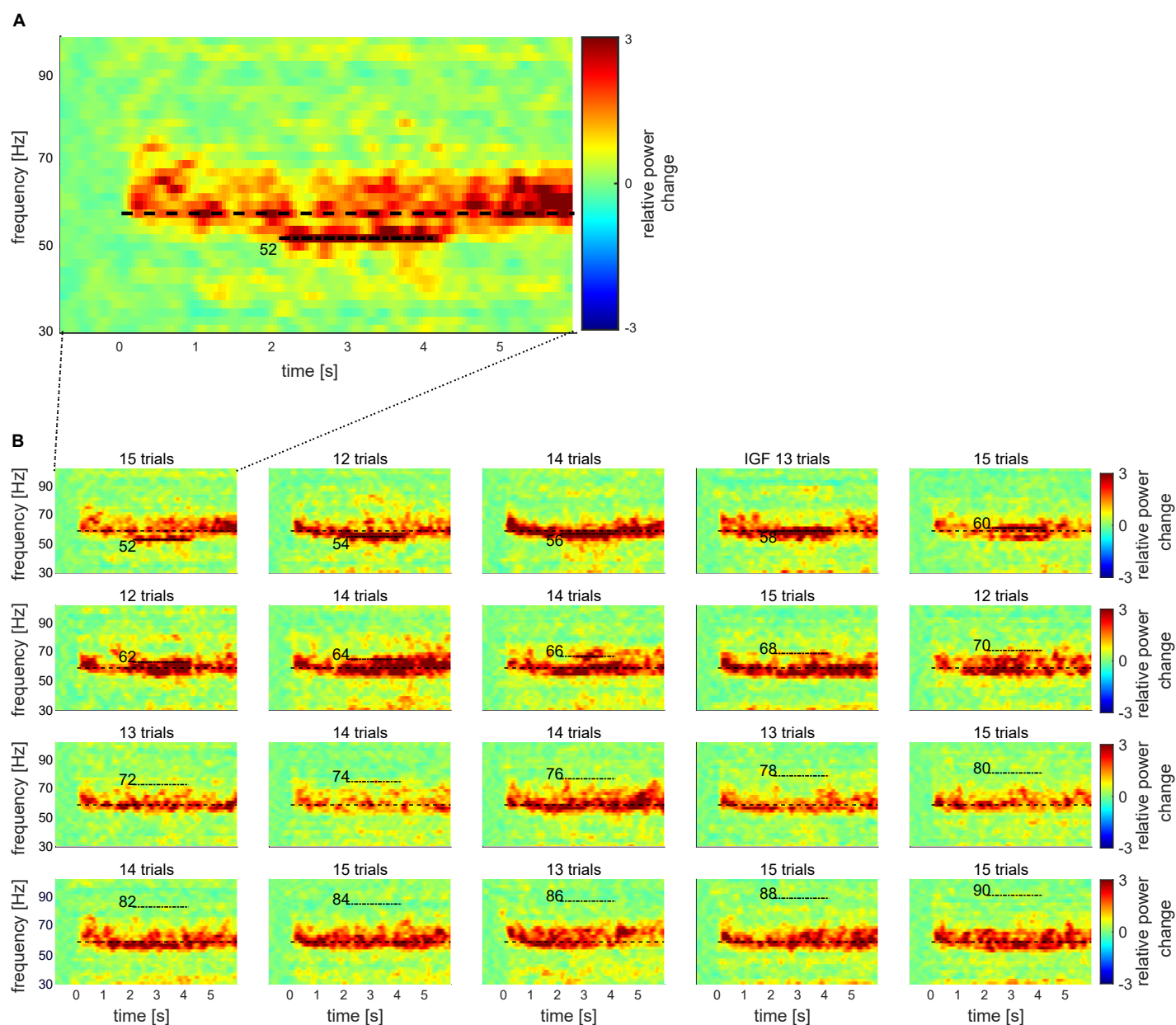
Figure 5: The time-frequency representations (TFRs) of power for one representative subject, showing relative power change averaged over trials and SOIs in the *flicker&gratings* condition. **A** Photic drive at 52 Hz. The moving grating stimuli were presented for 0 - 6 s whereas the flicker was a applied from 2 to 4 s. Sustained gamma-band activity is clearly observable throughout the presentation of the stimuli, with a power increase of 3 relative to baseline. Additionally, the rhythmic stimulation elicited a response at 52 Hz, which seems to coexist with the gamma oscillations, indicating that the photic drive is unable capture the dynamics of the gamma oscillation. **B** The plots for the frequencies from 52 to 90 Hz. Stimulation frequencies and IGF (here 58 Hz) are indicated by horizontal dashed lines. The flicker induced responses up to 66 Hz in this participant. Gamma oscillations persist in presence of flicker responses, suggesting that they coexist.

165    The group averaged, aligned TFRs are shown in Figure 6 for frequencies ranging from IGF-6 Hz to

166    IGF+16 Hz. The endogenous gamma oscillations are observed as the power increase extending from 0 - 6

167    s, and the flicker response as the power change in the 2 - 4 s interval marked by dashed lines, respectively.

168    The photic stimulation induces a reliable response that decreases toward 12 Hz above the IGF. Despite the

169    representation of the gamma oscillations being smoothed due to inter-individual differences, the averaged

170    aligned TFRs of power support the observations in the single subject data: both the gamma oscillations and

171    flicker response coexist in the 2 - 4 s interval. Furthermore, there is no indication of the gamma power being

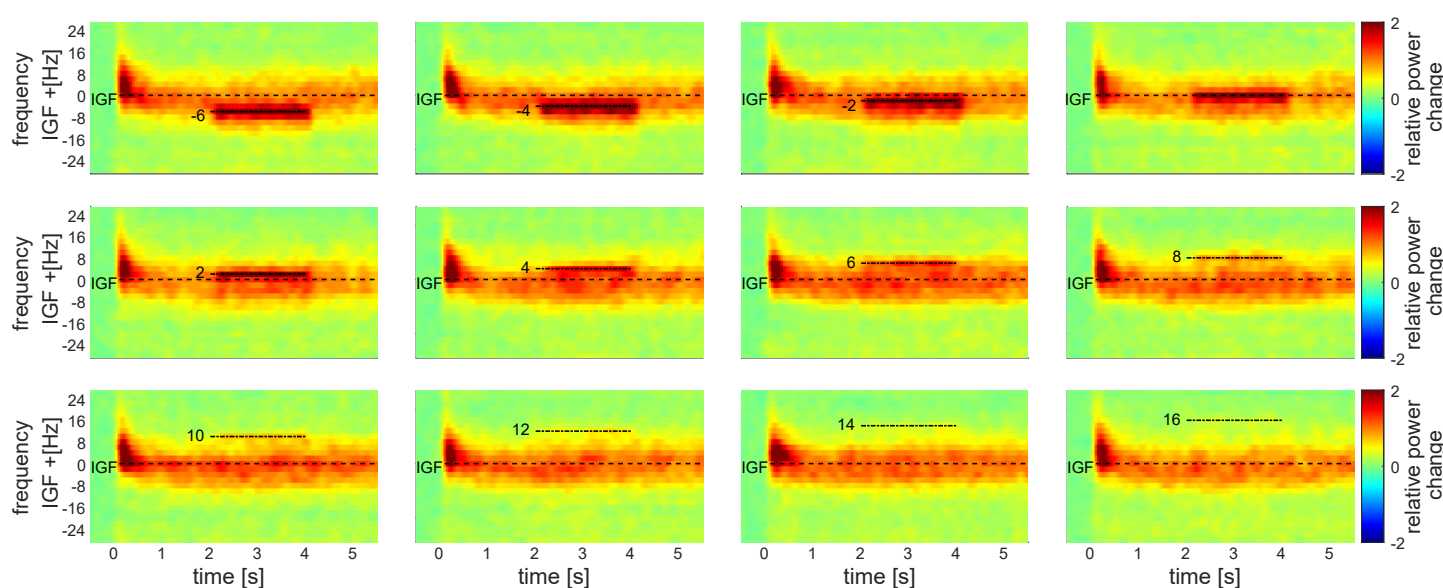172    reduced during RFT at frequencies close to, but different from, the IGF.



Figure 6: Grand-average TFRs of power after aligning to the IGF for each subject in the *flicker&gratings* condition. The stimulation frequencies (from -6 to 16 Hz relative to the IGF) are indicated by dashed horizontal lines. As suggested by the single subject TFRs in Figure 5, the endogenous gamma oscillations and the flicker response seem to be coexistent. Thus, there is no obvious indication of the photic drive being able to capture the dynamics of the gamma oscillations.

**No evidence that the oscillatory gamma dynamics can be captured by frequency entrainment**

174    Synchronisation of neuronal oscillations by rhythmic stimulation could be conceptualised as the entrainment

175    of a self-sustained oscillator by an external force (e.g. Notbohm et al., 2016; Helfrich et al., 2019). A central

176    assumption of this phenomenon is the existence of a 'synchronisation region' in the frequency range around

177    the endogenous frequency of the oscillator, the so-called Arnold tongue (e.g. Pikovsky et al., 2003). Driving

178    frequencies falling inside this synchronisation region, will be able to modulate the dynamics of the self-

13

sustained oscillator (also see Hutt et al., 2018). With this in mind, we investigated the power of the gamma oscillations before and during the photic drive for frequencies in the vicinity of the IGF (Figure 7) in the *flicker&gratings* condition. For each participant, we considered the relative power change induced by the moving gratings in the 0.5 - 1.5 s interval (T1) before the flicker onset and in the 2.5 - 3.5 s interval (T2) in which both the moving gratings and the photic drive were present. We investigated this for stimulation frequencies below the IGF (averaged power for -6 and -4 Hz) and above (averaged power for +4 and +6 Hz). Assuming a symmetric Arnold tongue centred at the IGF, as shown for entrainment in the alpha-band (Notbohm et al., 2016), we expected a reduction in power at the IGF in interval T2 for both higher and lower driving frequencies, i.e. an effect of time, but not frequency. Figure 7A depicts power change at the IGF for the factors stimulation frequency (drive<IGF and drive>IGF) and time interval (T1 and T2), averaged over the SOIs for each subject. In accordance with the TFRs in Figure 6, there is no meaningful indication for gamma power being reduced during the T2 interval as compared to the T1 interval, affirming the coexistence of the two responses. Surprisingly, power at the IGF seems to be slightly enhanced at T2 for drive>IGF. Indeed, a factorial repeated-measures ANOVA on the factors *time* and *frequency* did not reveal any significant main effects. However, there was a significant interaction effect of *interval* (T1 vs T2) and *frequency* (drive<IGF vs drive>IGF) ($F(1, 21) = 5.09, p = 0.003**, \eta^2 = .003$), which was unexpected based on the assumption of a symmetrical synchronisation area around the IGF. A post-hoc dependent sample t-test, comparing power change at T2 relative to T1 for drive<IGF and drive>IGF (see Figure 7B) indicated that the interaction was driven by the increased gamma power during drive>IGF, $t(21) = -2.44, p = 0.012*, 95\%CI = [-Inf - 0.029], r = .22$. Importantly, we were unable to find the expected reduction in gamma power during rhythmic photic stimulation, i.e. there was no indication that the rhythmic drive was capturing oscillatory gamma dynamics.
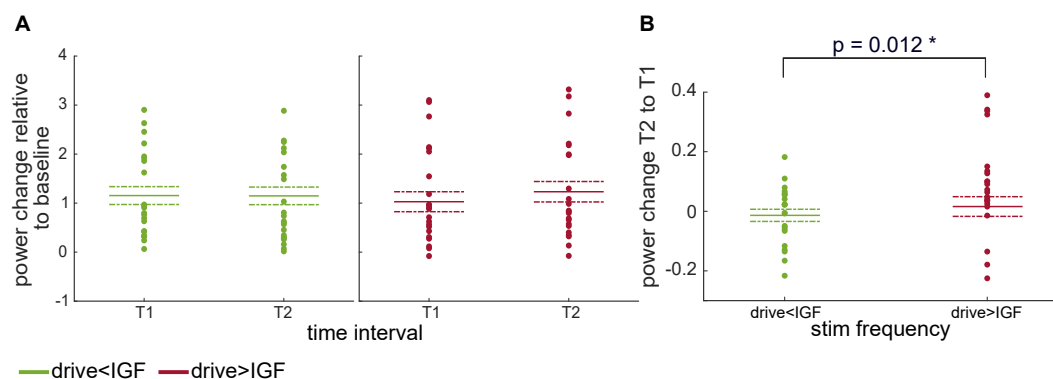
14

Figure 7: **A** Power change relative to baseline at IGF in response to the moving grating stimuli before (T1; 0.5 - 1.5 s) and during application of the flicker (T2; 2.5 - 3.5 s), at frequencies below and above IGF (drive<IGF [-6, -4 Hz] and drive>IGF [+4, +6 Hz], respectively). Scatters demonstrate individual values, solid and dashed lines depict mean and standard errors, respectively. The key finding is that power at T2 is not decreased compared to T1 for either of the frequency ranges. Instead, the plots show a slight increase in power at T2 for drive>IGF. A repeated measures ANOVA indicates a significant interaction of frequency and interval ($F(21, 1) = 5.09, p = 0.003**, \eta^2 = .003$), but no main effect of time interval. **B** Power change at T2 relative to T1, for flicker frequencies below and above IGF. A post-hoc dependent sample t-test reveals that the interaction in **A** was driven by a significant increase of IGF power during the photic drive at frequencies just above IGF, ($t(21) = -2.44, p = 0.012*, r = .22$).

## Photic drive does not reliably modulate gamma phase

Synchronisation of a self-sustained oscillator by an external force, i.e. entrainment, is reflected by a constant phase angle between the two oscillators over extended intervals, so-called *phase plateaus*. These might occur when the frequency of the driver is close to the endogenous frequency of the oscillator, i.e. within its Arnold Tongue (Tass et al., 1998; Pikovsky et al., 2003; Notbohm et al., 2016). When approaching the edge of the synchronisation region, episodes of constant phase angles are interrupted by so-called *phase slips* that emerge when the self-sustained oscillator briefly unlocks from the driving force and oscillates at its own frequency. These phase slips will be observed as steps between the phase plateaus. We implemented the phase plateau analysis to complement the PLV analysis in Figure 4, which quantifies the average synchrony between photodiode and neuromagnetic signal over trials, but is not able to identify intermittent plateaus. If the photic drive entrains endogenous gamma oscillations, strong phase locking is expected, reflected by phase plateaus sustained over the duration of at least one cycle of the flicker frequency. These would be particularly pronounced during stimulation at and close to the IGF in the *flicker&gratings* condition, due to the

15

214 presence of the self-sustained gamma oscillator, but not in the *flicker* condition. To investigate phase entrain-

215 ment of the gamma oscillations by the photic drive, we inspected the phase angle between the photodiode

216 and one, individually selected, occipital gradiometer of interest per participant. Time series of phase per

217 trial were estimated separately for the two signals, using a sliding time-window Fourier transform approach

218 ($\Delta$T = 3 cycles = $3/f_{flicker}$s; Hanning taper). Phase differences per trial were obtained by subtracting the

219 unwrapped phase angle time series in the two sensors.

220 *Phase angle between photodiode and MEG signal over time*   Figure 8 illustrates the unwrapped phase

221 angles between the MEG and photodiode signal during the photic drive at the IGF (here 58 Hz), in the *flicker*

222 (A) and *flicker&gratings* condition (B), respectively, for the same representative participant shown in Figure

223 1A, 2A and 5. Each coloured line graph depicts an individual trial. In both conditions, the MEG signal drifts

224 apart from the photic drive, towards a maximum difference of 60 radians, i.e. a phase difference of about

225 9.5 cycles, by the end of the trial (A and B, top panel). Interestingly, the direction of the phase angle appears

226 to change during some of the trials, suggesting spectral instability of the gamma oscillations. Furthermore,

227 the graphs demonstrate a substantial inter-trial variability. This diffusion between trials, quantified for each

228 participant as the standard deviation over trials at the end of the photic stimulation (t=2 in *flicker* and t=4

229 in *flicker&gratings* condition), converted from radiant to ms, is juxtapositioned in Figure 8C for the two

230 conditions. It can be readily seen that the phase angles between the stimulation and MEG signal fan out

231 highly similarly in absence and presence of the endogenous gamma oscillations.

232 *Phase plateaus*   Visual inspection of the first 0.25 s of the phase angle times series, depicted in Figure

233 8A,B lower panel, does not suggest a comparably high number of phase plateaus in the *flicker&gratings*

234 condition, that would have been expected if the photic drive was able to entrain the endogenous gamma

235 oscillator. Importantly, the graphs demonstrate the phase angles to reach values of over $2\pi$, i.e. more than

236 one cycle, within the duration of the first gamma cycle (17.2 ms), suggesting that even stimulation at the

237 endogenous frequency of the oscillator cannot capture the gamma dynamics. To verify these observations

238 for the entire sample, plateaus during stimulation at the IGF were identified based on the mean absolute gra-

239 dient ($\leqslant$0.01, see equation 3) over the duration of one cycle of stimulation, i.e. 18 consecutive samples for a

240 flicker frequency of 58 Hz. Figure 8D shows the average number of plateaus per trial as a function of flicker

16

241  frequency aligned to IGF, averaged over participants. Again, the shaded areas indicate the standard error.

242  While the *flicker&gratings* condition exhibits more phase plateaus than *flicker* for all stimulation frequen-

243  cies, the number of plateaus decreases similarly in both conditions with increasing frequency. Importantly,

244  stimulation at the IGF did not result in the highest number of plateaus in either condition. The results affirm

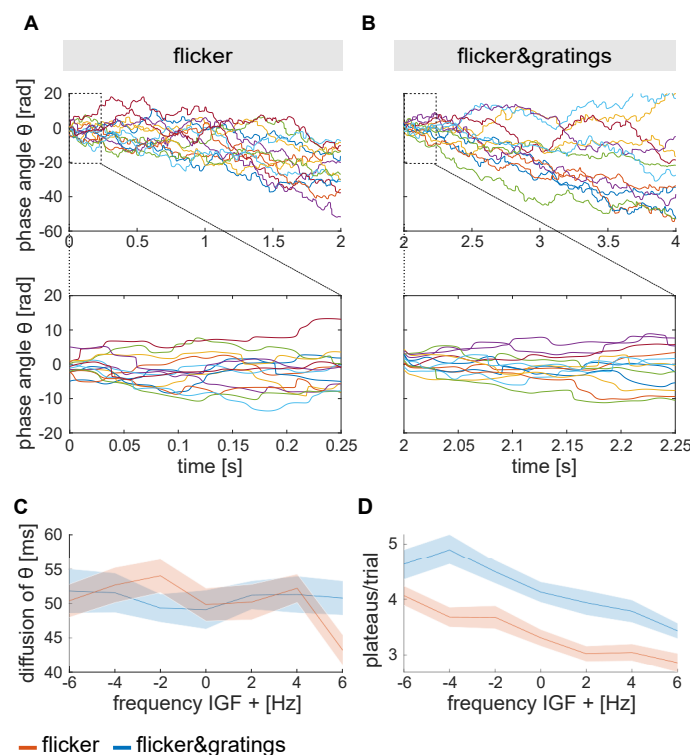245  the observations presented in Figure 4A and B.

Figure 8: **A,B** Phase angle between photodiode and the MEG signal (one gradiometer of interest) at the IGF, for one representative participant; coloured lines depict individual trials. **A** Phase angle $\theta$ in the *flicker* condition over duration of the flicker presentation (upper panel) and the first 250 ms (lower panel). The MEG signal drifts apart from the stimulation and can reach a maximum accumulated phase difference of 60 rad, i.e. 9.54 cycles, at the end of the stimulation and up to 15 rad, i.e. 2.39 cycles, in 250 ms. **B** The increase in phase difference over the time of the stimulation for the *flicker&gratings* condition (upper panel) and in the first 250 ms (lower panel). The diffusion of the phase difference across trials is similar to the *flicker* condition. Moreover, there is no clear difference in the number and length of phase plateaus between conditions, implying that the presence of the gamma oscillations does not facilitate entrainment at the IGF. **C** Fanning out across trials as a function of frequency aligned to IGF. Trials diffuse to a highly similar extent in both conditions and across frequencies. **D** Number of plateaus per trial as a function of frequency. While the *flicker&gratings* conditions exhibits more plateaus for all flicker frequencies, there is no indication that stimulation at the IGF results in comparably strong synchronisation.

18

### The sources of the gamma oscillations and the flicker response peak at different locations

The coexistence of the endogenous gamma oscillations and flicker response suggest that these two signals are generated by different neuronal populations; possibly in different regions. To test this assumption we localised the respective sources using Linearly Constrained Minimum Variance spatial filters (LCMV; Veen et al., 1992), estimated based on the data of the -0.75 to -0.25 baseline and the 0.25 to 1.75 s stimulation intervals in both conditions. Note that for each participant, one common filter was used for source estimation in both conditions. Power values at the IGF and flicker frequencies, averaged up to 78 Hz, respectively for the *flicker&gratings* and *flicker* condition, were extracted, and relative power change was computed at each of the 37,163 dipole locations using equation 1. Figure 9 illustrates the grand-average of the source localisation for the gamma oscillations (A) and flicker response (B). Consistent with previous work, both responses originate from mid-occipital regions (Hoogenboom et al., 2006; Zhigalov et al., 2019). Interestingly, the peak location of the endogenous gamma oscillator was significantly inferior to the flicker response (dependent sample t-test $t(21) = -5.12, p = 2.29e - 5***, r = .55, 95\% \ CI = [-Inf - 5.67]$, see Figure 9C and D). Indeed, using the MNI to Talaraich mapping online tool by Biomag Suite Web (MNI2TAL Tool) (see Lacadie et al., 2007, 2008), the centre peak of the gamma oscillations was located in the left secondary visual cortex (V2, Brodmann area 18; MNI coordinates = [-6mm -96mm -8mm]), while the peak of the flicker response was at a two millimetre distance to the primary visual cortex (V1, Brodmann area 17; MNI coordinates [6mm -96mm 4mm]). It should be noted, however, that using MRIcroGL, with the Automated Anatomical Labelling atlas 3 (AAL3) (Rolls et al., 2020), the anatomical landmarks of the gamma oscillations and flicker responses were identified in the left and right Calcarine fissure (and surrounding cortex), respectively, which is considered to mainly cover the primary visual cortex (Johns, 2014). Crucially, while the sources of the gamma oscillations and the flicker response overlap to some extend, they peak in distinguishable locations in occipital regions.
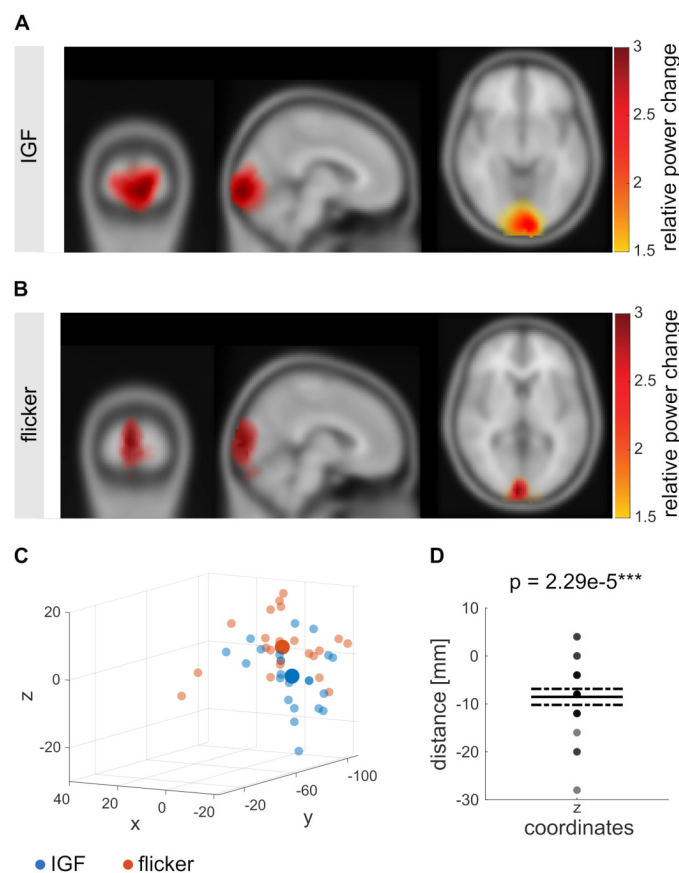
Figure 9: Source estimates using the LCMV beamformer approach mapped on a standardised MNI brain. **A** Source estimation of the visually induced gamma oscillations, with the peak of the source identified at MNI coordinates [0mm -98mm -7mm]. **B** Source estimation of the flicker response, with the average peak source at [3mm -96mm 2mm]. **C** Coordinates of the peak sources for all participants (small scatters) and grandaverage (large scatters) for the *flicker&gratings* and *flicker* condition (blue and orange, respectively), indicating that the gamma oscillations peak in brain areas inferior to the flicker response. **D** Difference between the z-coordinates (inferior-superior axis) of the peaks of the sources in both conditions, demonstrating an average difference of 8.5mm. A dependent sample t-test confirms this distance to be significant, $t(21) = -5.12, p = 2.29e - 5***, r = .55, 95\% CI = [-Inf - 5.67]$.

## Discussion

In this MEG study, we explored resonance properties and entrainment of the human visual system to a rapid photic drive >50 Hz in the absence and presence of endogenous gamma oscillations. Strong, sustained gamma oscillations were induced using moving grating stimuli (Hoogenboom et al., 2006, 2010; Van Pelt & Fries, 2013; Muthukumaraswamy & Singh, 2013). This allowed us to identify the individual gamma frequency in each participant. The photic drive induced responses for frequencies up to ~80 Hz, both in presence and absence of grating-induced endogenous gamma oscillations. To our surprise, we did not find evidence for resonance, i.e. an amplification of an individually preferred frequency in the range of the rhythmic stimulation, in either condition, despite the endogenous gamma rhythms being above 50 Hz in all participants. Moreover, there was no indication that the endogenous gamma oscillations synchronised with the rhythmic stimulation, i.e. no evidence for entrainment. Instead, the flicker response and the visually induced gamma-band activity appeared to coexist. Indeed, source estimation using Linearly Constrained Minimum Variance (LCMV) spatial filters (Veen et al., 1992), suggests that the neuronal sources of the flicker response and the endogenous gamma oscillations peak at distinct locations in visual cortex.

### Endogenous gamma oscillations and flicker response might be generated by different populations

*Low-pass filter properties of the visual system might hinder entrainment* While the sources of the gamma oscillations and the response to the (nearly) invisible flicker did overlap in occipital cortex, their peak coordinates were found to be significantly different. Furthermore, the MNI2TAL online tool (see Lacadie et al., 2007, 2008) indicates that the two responses peak in different Brodmann areas, namely the primary (V1) and secondary visual cortex (V2), suggesting that the flicker response was unable to impact activity in visual cortex beyond V1. Several studies have considered the filter properties of different stages in the visual hierarchy of the mammalian brain (Cormack, 2005), i.e. retinal ganglion cells (e.g. Kuffler, 1953), lateral geniculate nucleus (LGN) of the thalamus and the primary visual cortex (e.g. Hawken et al., 1996; Carandini et al., 1997; Cormack, 2005; Ringach, 2004; Sharpee et al., 2006). The low-pass filter properties of the thalamus (Connelly et al., 2015) might have attenuated the photic drive in our data at frequencies above 80 Hz, leading to no measurable responses in this range. Interestingly, Hawken et al. (1996) found

296   low-pass filter properties at about 20 Hz in V1 in the projections from granular input layers (L4a, 4c$\alpha$ and

297   4c$\beta$) to supragranular (L2/3, 4b) and infragranular layers (L5,6) (also see Douglas & Martin, 2004; Fröhlich,

298   2016). Thus, the imposed flicker response might not travel beyond the granular layer of V1 and thus does

299   not impact higher order visual areas, such as V2. This is supported by intracranial recordings in macaques

300   which identified the strongest gamma synchronisation in response to drifting grating stimuli in V1 in supra-

301   granular layers (L2/3 and 4B) (Xing et al., 2012), whereas steady-state responses to a 60 Hz photic flicker

302   were localised in granular layer 4c$\alpha$ (Williams et al., 2004).

303   *Limitations of the source estimation*   It should be noted that the source localisation shown in Figure 9A

304   and B represents an estimated location of the neuronal populations from which the two responses emerge.

305   Moreover, while the neuromagnetic signal at locations inside the head can be estimated with a limited set of

306   parameters (forward problem), there is no unique solution to describe the electromagnetic sources outside

307   the skull (inverse problem) (Baillet, 2013). Therefore, interpretations of sources of neuromagnetic signals

308   recorded with MEG should be interpreted tentatively. Also note that, besides the peak source, the localisation

309   of the gamma oscillations also includes inferior and mid-occipital regions covering primary and secondary

310   visual cortex. Indeed, in previous work, the origins of the grating-induced gamma oscillations have been

311   found in both V1 and V2 (Hoogenboom et al., 2006, 2010, but see Buffalo et al. 2011; Roberts et al. 2013

312   for intra-cranial recordings in non-human primates). Again, it should be acknowledged that MRIcroGL

313   used with the AAL3 atlas (Rolls et al., 2020) indicates that both the gamma oscillations and flicker response

314   emerge from Calcarine regions. Furthermore, due to the spectral width of the gamma oscillations (see Figure

315   1C), we were unable to localise the flicker response in the *flicker&gratings* condition without confounds

316   with the endogenous oscillator. Despite the concerns outlined above, we found a systematic difference

317   between the sources of the two oscillatory activities: the source of the gamma oscillations was found to

318   be significantly inferior to the flicker response. Pairing the current paradigm with intracranial recordings

319   in non-human primates would enable to test the reliability of this observation with higher spatial precision.

320   Alternatively, computational models, as the one demonstrated by Lee & Jones (2013), would be suitable to

321   investigate whether the grating-induced gamma oscillations and flicker response are likely to be generated

322   by different neuronal populations.

22

## No evidence for resonance at Individual Gamma Frequencies

Adaikkan et al. (2019) demonstrate compelling evidence for a visual flicker at 40 Hz to modulate neuronal responses, to strengthen synapses and to protect neurons and non-neuronal cells from degeneration, in rodents. These effects have been attributed to a synchronisation of endogenous gamma oscillations with the photic drive. In parallel to that, in human subjects, systematic analyses of steady-state responses to rhythmic flickering lights at a broad frequency range from 1-100 Hz (Herrmann, 2001) and 3-80 Hz (Gulbinaite et al., 2019) have revealed amplified responses to stimulation at ∼40 and ∼47 Hz. These findings at first suggest that oscillatory activity in the gamma-band can be driven by photic stimulation. However, while these studies demonstrate resonance properties of the human visual system in the lower gamma band, they do not demonstrate entrainment of endogenous oscillations. We hypothesised the resonance properties of the visual system to be particularly pronounced when endogenous gamma oscillation were induced, resulting in amplified responses to a photic drive at the IGF. Yet, we did not find evidence for the endogenous gamma oscillator to resonate to the photic drive. It is uncertain whether neuronal gamma oscillations in the human brain are more difficult to target with sensory stimulation than the rodent brain, e.g. due to differences in cell-type expressions, and their laminar distribution (Hodge et al., 2019). Alternatively, our findings might be specific to grating-induced gamma oscillations that have been shown to vary with size and contrast of the stimuli (Schadow et al., 2007; Muthukumaraswamy & Singh, 2013; Perry et al., 2013; Orekhova et al., 2015). Furthermore, it has been pointed out that such strong, narrow-band gamma oscillations are only reliably induced by gratings, but not all visual stimuli, suggesting that they are generated by specialised neuronal circuits (Hermes et al., 2015). It remains to be investigated whether our results generalise to gamma oscillations in different (and broader) frequency-bands that are associated with different functional properties (see Colgin et al., 2009; Ray & Maunsell, 2011; Buzśaki & Wang, 2012). Again, laminar recordings in non-human primates would allow conclusions about whether the neuronal populations receiving the photic input are able to converge to the neurons engaging in the endogenous gamma oscillations. Crucially, the results of the presented study imply that targeting endogenous gamma oscillations using sensory stimulation is not trivial.

**Overlap of flicker and grating induced gamma oscillations**

Gamma-band synchronisation in monkey area V4 has been shown to predict reaction times to a behaviourally relevant stimulus in a visual attention task (Womelsdorf et al., 2006). Similarly, in humans, both the gamma oscillations induced by a moving grating stimulus (Hoogenboom et al., 2010) and gamma-band flicker responses (F. Bauer et al., 2009) have been reported to accelerate target detection, suggesting them to tune and organise neuronal responses in a similar way. It remains to be identified whether these functionally and spectrally similar oscillations can be generated by distinct neuronal populations with no anatomical overlap. In that case, a rapid photic drive might not be feasible to probe the causal role of gamma oscillations, but it can be applied to modulate behaviour or for therapeutic purposes. Indeed, M. Bauer et al. (2012) have reported that while a 60 Hz influences drive perceptual processing, these effects appear to be independent of the stimulation phase; suggesting that they cannot be explained by an entrainment of endogenous oscillations.

**Spectral precision of the individual gamma frequencies**

The sliding time window approach paired with a 500ms Hanning taper, applied in the time-frequency analysis, induced spectral smoothing of $\pm 3$ Hz. Consequently, the estimated IGFs are unlikely to perfectly match the true peak frequency of the endogenous gamma oscillator. Moreover, the stimulation frequencies were chosen to have a resolution of 2 Hz which further might result in the true gamma peak frequency being missed by the photic drive. Studies investigating entrainment in the alpha (Notbohm et al., 2016) and beta-band (Hanslmayr et al., 2014) in human subjects have demonstrated modulating effects on neuronal oscillations for stimulation rhythms within the range of the endogenous frequencies $\pm 1$ Hz. Moreover, the natural peak of the identified gamma frequencies extends over a frequency range of about 10-16 Hz (IGF $\pm 5$-8 Hz), indicating that it should cover about 4 stimulation frequencies for each participant. Therefore, we conclude that the frequency resolution in this study does not explain the lacking evidence for entrainment. Our findings are contrasted by studies on visual entrainment of neuronal alpha oscillations (Schwab et al., 2006; Spaak et al., 2014; Notbohm et al., 2016; Fiene et al., 2020), which have been reported to emerge from infragranular (Spaak et al., 2012) as well as supragranular layers (Haegens et al., 2015; Dougherty et al., 2017). While our results do not support entrainment of oscillations in the gamma-band, these studies

376  show that it is indeed possible to entrain oscillations at lower frequencies.

## Concluding remarks

378  Our results suggest that rapid photic stimulation does not entrain endogenous gamma oscillations and can

379  therefore not be used as a tool to probe the causal role of gamma oscillations in cognition and perception.

380  However, the approach can be applied in Rapid Frequency Tagging (RFT) to track neuronal responses with-

381  out interfering, for instance, to investigate covert spatial attention (Zhigalov et al., 2019) and multisensory

382  integration (Drijvers et al., 2020, bioRxiv).

# Materials and Methods

## Experiment

### Experimental Procedure & Apparatus

386  The MEG data were recorded using a MEGIN Triux system housed in a magnetically shielded room (MSR;

387  Vacuumschmelze GmbH & co., Hanau, Germany). Neuromagnetic signals were acquired from 204 orthog-

388  onal planar gradiometers and 102 magnetometers at 102 sensor positions. Horizontal and vertical EOG,

389  the cardiac ECG signals, stimulus markers as well as luminance changes recorded by a photodiode (see

390  below) were acquired together with the neuromagnetic signal. The data were lowpass filtered online at 330

391  Hz and sampled at 1000 Hz. Structural magnetic resonance images (MRIs), for later co-registration with

392  the MEG data, were acquired using a 3 Tesla Siemens MAGNETOM Prisma whole-body scanner (Siemens

393  AG, Muenchen, Germany), TE = 2 ms, and TR = 2 s). For two subjects, the T1-weighted images obtained

394  in previous experiments, using a 3 Tesla Philips Achieva Scanner (Philips North America Corporation, An-

395  dover, USA), were used (scanned at the former Birmingham University Imaging Centre). Participants were

396  invited to two separate sessions during which the MEG data and the anatomical images were acquired, re-

397  spectively. Whenever possible, the MEG recording preceded the MRI scan; otherwise, the MEG session

398  was scheduled at least 48 hours after the MRI session to avoid any residual magnetisation from the MRI

399  system. Volunteers were requested to remove all metal items (e.g. jewellery) before entering the MSR. To

400  enable later co-registration between MRI and MEG data, four to five head-position-indicator (HPI) coils

401  were attached to the participants' foreheads. Along with the position of the coils, three fiducial landmarks

(nasion, left and right tragus) and over 200 head-shape samples were digitized using a Polhemus Fastrak (Polhemus, Colchester, USA). Following the preparations, the participants were seated in upright position under the dewar, with orientation set to 60°. The MEG experiment consisted of fifteen blocks lasting 4 min 30 s each. Participants were offered breaks every ∼20 min but remained seated. At the beginning of each of these recording blocks, subjects were instructed to sit with the top and backside of their head touching the sensor helmet. The positions of the HPI coils relative to the sensors was gathered at the beginning of each recording block, but not continuously. The MEG experiment lasted ∼75 min in total.

**Rapid photic stimulation**

Stimuli were presented using a Propixx lite projector (VPixx Technologies Inc, Saint-Bruno, QC Canada) which allows refresh rates of up to 1440 Hz. To achieve this high-frequency mode, the projector separates the screen (initial resolution: $1920 \times 1080$ pixels) into quadrants and treats them as separate frames, resulting in a display resolution of $960 \times 540$ pixels. The RGB colour codes for each quadrant, viz. red, green and blue, are converted to a greyscale, separately for each frame and colour, and presented consecutively within one refresh interval. The resulting twelve frames that are presented at a refresh rate of 120 Hz, i.e. $12 \times 120$ Hz = 1440 Hz. This approach allows to drive the luminance of each pixel with high temporal precision, allowing for smooth sinusoidal modulations, reducing unwanted harmonics (see Figure 10C,D). In this study, we applied rapid rhythmic stimulation at frequencies ranging from 52 to 90 Hz in 2 Hz increments.

**Experimental Paradigm**

Stimuli were created in MATLAB 2017a (The MathWorks, Inc. Natick, MA, USA) and presented using the Psychophysics Toolbox Version 3 (Brainard, 1997).

*Conditions* The experiment consisted of two conditions that will be referred to as the *flicker* and the *flicker&gratings* condition, respectively. Each trial began with a one-second interval, in which a central white fixation cross was presented on a dark grey background. In the *flicker* trials, a circular patch of size 6.47° was presented for 2 s. Its luminance was modulated sinusoidally at frequencies between 52 and 90 Hz (Figure 10A). Frequencies were randomised and balanced across trials. The patch was centred on the fixation cross, such that it was presented both foveally and parafoveally (Van Pelt & Fries, 2013, and see *Task & Time Course*). To minimise the visibility of the flicker, the mean luminance of the patch was matched

26

429   to the background (33% luminance, RGB [84 84 84]). Each trial ended with a two-second interval in which

430   only the fixation cross was presented.

431   In the *flicker&gratings* condition, the baseline interval was followed by a 2 s presentation of a moving

432   grating stimulus that has been shown to reliably elicit gamma oscillations in the visual cortex (e.g. Hoogen-

433   boom et al., 2006, 2010; Muthukumaraswamy & Singh, 2013; Tan et al., 2016). The stimulus was the same

434   size as the patch (6.47°) and had a spatial frequency of 2.93 cycles/° (see Figure 10B). The rings contracted

435   towards the centre of the screen with a velocity of 1.06 °/s, i.e. 2.05 cycles/s. In the subsequent 2 s in-

436   terval, the stimulus was flickered at the respective frequencies, followed by another 2 s interval in which

437   the concentric moving circles remained on screen without photic stimulation. Note that the modulation of

438   the luminance can only be applied to non-black tones and therefore only the grey rings of the grating were

439   flickered. To keep the overall brightness of the stimulation similar between conditions, the luminance of the

440   circular patch in the *flicker* condition ranged from 0 to 66% (of maximum luminance), while the brightness

441   of the gratings in the *flicker&gratings* ranged from 33 and 99%. The flicker was applied to a small circular

442   patch in the lower right corner of the screen, to acquire the stimulation signal with a photodiode.

443   *Task & Time Course*   Participants were kept vigilant by performing a simple visual detection task that

444   required them to respond to a 45° rotation of the fixation cross at the centre of the screen, which occurred

445   once every minute (e.g. Zaehle et al., 2010). Data including the target and/or the responses were discarded

446   and not considered in the analysis. The rotation took place after a trial in the majority, i.e. 60%, of the

447   cases. The remaining 40% of rotations took place at any point during a trial. The experiment was divided

448   into 15 blocks of 4.5 min, resulting in a recording time of 75 min in total. Within one block, each of the

449   twenty stimulation frequencies were applied in both conditions, in randomised order. Thus, every block

450   consisted of 40 frequency× 2 condition combinations, resulting in a total of 15 repetitions of each of these

451   combinations (i.e. 15 trials per flicker frequency for each of the two conditions). To minimise the amount of

452   trials rejected by eye-blink artefacts, 3 s breaks, indicated by a motivating catchphrase or happy face on the

453   screen, were incorporated every five trials, i.e. every 25 - 35 seconds. Participants were instructed to utilise
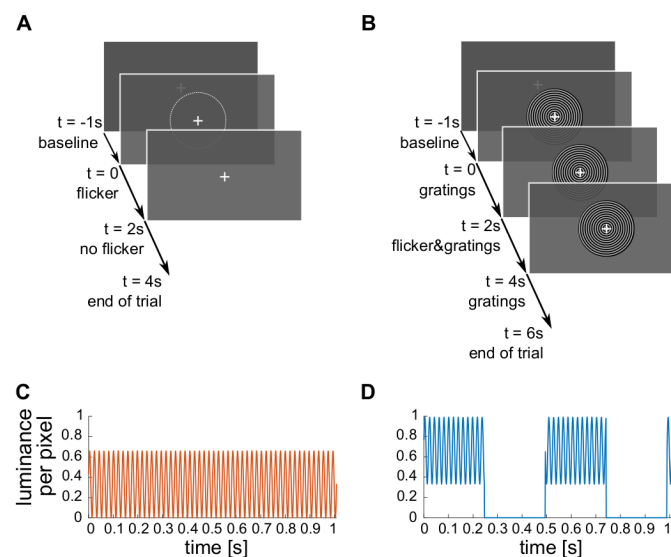
454   these breaks to rest their eyes.

Figure 10: The experimental paradigm. **A** Trials in the *flicker* condition. A 1 s baseline interval with a central fixation cross was followed by a 2 s interval of the rapid flicker applied to circular patch of size 6.47°. The average luminance in the flickering patch was equal to the surrounding grey colour, making the flickering patch almost unperceivable. The trials ended with 2 s of the fixation cross only. **B** The trials in the *flicker&gratings* condition. The 1 s baseline interval was followed by 2 s of grating stimuli presented centrally on the screen, contracting inwards. Subsequently, the flicker was imposed onto the stimuli for 2 s. The trial ended with a 2 s presentation of the moving gratings without photic stimulation. **C** Sinusoidal luminance change in one pixel induced by the photic drive at 52 Hz in the *flicker* condition. **D** Luminance change in one pixel as a result of the flicker and the gratings moving concentrically with a velocity of 2.05 cycles/s. To maintain a similar mean luminance between conditions, photic modulation of the invisible patch in **A** ranged from 0 to 66% (mean RGB [84 84 84]), while the light grey rings of the grating, that is 50% of the stimulus' surface, were flickered between 33 and 99% (mean RGB [168 168 168] per ring).

## Participants

456 This project was reviewed and approved by the local Ethics Committee at University of Birmingham, UK.

457 Thirty-one students of the University of Birmingham participated in the experiment. One experimental

458 session was terminated prematurely due to the participant not being cooperative, resulting in a sample of

459 thirty participants (15 female), aged 25.7 ± 3.4 years. This sample size was decided upon based on a

460 conceptually similar study investigating entrainment of neuronal alpha oscillations by Notbohm et al. (2016).

461 All volunteers declared not to have had a history of neuropsychiatric or psychological disorder, reported to

462 be medication-free and had normal or corrected-to-normal vision. For safety reasons, participants with metal

463 items inside their bodies were excluded at the selection state. Prior to taking part in the study, participants

464 gave informed consent, in accordance with the declaration of Helsinki, to both the MEG recording and the

465 MRI scan and were explicitly apprised of their right to abort the experiment at any point. The reimbursement

466 amounted to £15 per hour. To allow analysis of flicker responses at frequencies with a sufficient distance to

467 the individual gamma frequency (IGF; see ) of the participant, i.e. ±6 Hz, 8 participants were excluded due

468 to their IGF being below 58 Hz. Thus, the data of 22 participants were included in the following analyses

469 (11 female; mean age 25.7 years).

## Data Analysis

471 Analysis was performed in MATLAB 2017a and 2019b (The MathWorks, Inc. Natick, MA, USA) using

472 the fieldtrip toolbox (Oostenveld et al., 2011).

### Sensor Analysis

474 At the sensor level, the analysis was confined to the planar gradiometer signals, as these provided the best

475 signal-to-noise ratio.

476 *MEG preprocessing*    Trials containing the target or button presses were excluded. The data were read into

477 MATLAB as 5 s and 7 s trials for the *flicker* and *flicker&gratings* conditions, respectively. Artefactual

478 sensors were identified visually during and after the recordings for each participant, and interpolated with

479 the data of their neighbouring sensors (0 to 2 sensors per participant). The individual trials were linearly

480 detrended. Trials containing head movements and/or multiple eye blinks were discarded using a semi-

481 automatic approach. An ICA approach ('runica' implemeted in FieldTrip) was used to project out cardiac

482 signals, eye blinks and eye movement. The sensor positions relative to the HPI coils were loaded in from

483 the data files and averaged for each subject.

29

484 *Time-Frequency Representation of Power*    Time-Frequency Representations (TFRs) of power were calcu-

485 lated using a sliding time-window approach ($\Delta T = 0.5$ s; 0.05 s steps). A Hanning taper (0.5 s) was applied

486 prior to the Fourier-transform. This approach induced spectral smoothing of $\pm 3$ Hz. Relative power change

487 in response to the stimulation, i.e. the moving grating and/or the photic drive, was calculated as:

$$P_{\text{normalized}} = \frac{P_{\text{stim}}}{P_{\text{base}}} - 1 \tag{1}$$

488    with $P_{\text{stim}}$ being the power during stimulation and $P_{\text{base}}$ being the power in the baseline interval. The

489 baseline interval was 0.75 - 0.25 s prior to the onset of the flicker (*flicker* condition) or the moving grating

490 stimulus (*flicker&gratings* condition).

491 *Individual Gamma Frequency*    The frequency band of the oscillatory activity elicited in response to the

492 moving grating stimulus was identified individually per participant. TFRs of power were calculated for the

493 baseline interval and presentation of the moving grating in the *flicker&gratings* condition and averaged over

494 trials. The results were averaged over the 0.25 - 1.75 s interval, and the frequency bin with the maximum

495 relative power was considered the Individual Gamma Frequency (IGF). In the case of two maxima, the

496 average of the respective two frequencies was treated as the IGF. For each participant, the 4 to 6 gradiometers

497 with the strongest gamma response to the moving gratings were selected as the Sensors-of-Interest (SOI).

498 *Phase-Locking*    The average phase-synchrony between the photodiode (recording the visual flicker) and

499 the neuromagnetic signal at the SOI was quantified by the Phase-Locking Value (PLV) (Lachaux et al.,

500 1999; Bastos & Schoffelen, 2016) calculated using the 0.5 s sliding window multiplied with a Hanning

501 taper of equal length. The phases of both signals were calculated from Fourier transformations, applied to

502 the tapered segments. The PLV was computed separately for each *frequency$\times$condition*:

$$PLV = \frac{1}{n} \left| \sum_{n=1}^{N} exp(j\theta(t, n)) \right| \tag{2}$$

503 where $\theta(t, n) = \phi_{\text{m}}(t, n) - \phi_{\text{p}}(t, n)$ is the phase difference between the MEG (m) and the photodiode (p)

504 signal at time bin $t$ in trial $n$ (see Lachaux et al., 1999, p.195 and Figure 4 and 8).

505 *Phase difference as a measure of entrainment*  Additionally, we investigated changes in phase difference

506 between the photodiode and neuromagnetic signal over time for flicker frequencies of IGF±6 Hz, to identify

507 intervals of strong synchrony, so-called *phase plateaus*. MEG and photodiode signals ($\Delta$T = 3 cycles =

508 $3/f_{flicker}$s) were convolved with a complex Hanning taper using the sliding time window approach. Phase

509 angles were derived from the Fourier transformed time series, unwrapped and subtracted to estimate the

510 phase difference over time for each trial. Plateaus were defined as a constant phase angle (maximum average

511 gradient 0.01 rad/ms) over the duration of one cycle of the stimulation frequency:

$$\frac{\sum_{i=1}^{\Delta T}|\nabla\theta_i|}{n} \leqslant 0.01 rad/ms \tag{3}$$

512 with $\nabla\theta_i$ being the gradient, i.e. slope, of the phase angle between MEG and photodiode signal at a

513 given sample $i$ and $n$ being the length of the cycle in ms, rounded up to the next integer, e.g. 17 ms for a

514 flicker frequency of 60 Hz. While the PLV quantifies the average phase-similarity of the two signals over

515 trials, this approach allows to investigate to what extent the stimulation and the MEG signal align in terms

516 of phase-difference in a given time interval.

517 *Statistical Analysis*  Statistical Analysis was performed in RStudio Version 1.2.1355 (RStudio Inc., North-

518 ern Ave, Boston, MA; R version 3.6.1., The R Foundation for Statistical Computing).

519 **Source Analysis**

520 *MRI preprocessing*  The raw T1 weighted images were converted from DICOM to NIFTI. The coordinate

521 system of the participants' individual MRI was aligned to the anatomical landmarks using the head-surface

522 obtained from the MRI and the scalp shapes digitized prior to the recordings. Realignment was done au-

523 tomatically using the Iterative Closest Point (ICP) algorithm (Besl & McKay, 1992) implemented in the

524 FieldTrip toolbox and corrected manually as necessary. The digitised headshape of one participant, for

525 whom there was no anatomical image available, was aligned to a standardised template brain.

526 *Linearly Constrained Minimum Variance Beamforming*  The neuroanatomical origins of the visually in-

527 duced gamma oscillations in the *flicker&gratings* condition and the response induced by the photic drive in

528 the *flicker* condition were estimated using Linearly Constrained Minimum Variance spatial filters (LCMV;

529 Veen et al., 1992), implemented in the Fieldtrip Toolbox (Oostenveld et al., 2011). The MEG forward model

530 was calculated using single-shell head-models, estimated based on the aligned anatomical images, and an

531 equally spaced 4-mm grid, warped into MNI (Montreal Neurologic Institute) space (Nolte 2003, also see

532 Oostenveld et al., 2011; Stenroos et al., 2012); yielding 37,163 dipoles inside the brain. The pre-processed

533 data, epoched in 7 and 5-second trials for the respective conditions, were band-pass filtered at 50 to 92 Hz,

534 by applying second order Butterworth two-pass high- and low-pass filters. Segments of 0.5 s of the base-

535 line interval (0.75 - 0.25 s prior to stimulation) and stimulation interval (0.75 - 1.25 s after flicker/grating

536 onset) were derived from the filtered data. For each participant, a common covariance matrix for the 204

537 planar gradiometers was computed based on the extracted time series and used to estimate the spatial filter

538 coefficients for each dipole location, whereby only the direction with the highest dipole moment was con-

539 sidered. Data in the baseline and stimulation intervals were projected to source space by multiplying each

540 filter coefficient with the sensor time series. Fast Fourier Transforms of the resulting time series, multiplied

541 with a Hanning taper, were computed for each of the 37,163 virtual channels, separately for the baseline

542 and stimulation intervals, and averaged over trials. Relative power change at the IGF and flicker frequencies

543 was computed by applying equation (1) to the Fourier-transformed baseline and stimulation intervals. The

544 source-localised power change values at flicker frequencies up to 78 Hz were averaged to identify a common

545 source for the oscillatory response to the photic drive.

## Acknowledgements

554 **Conflict of interest statement:** The authors declare no competing financial or non-financial interest.

# References

Adaikkan, C., Middleton, S. J., Marco, A., Pao, P. C., Mathys, H., Kim, D. N. W., . . . Tsai, L. H. (2019). Gamma Entrainment Binds Higher-Order Brain Regions and Offers Neuroprotection. *Neuron*, *102*, 929–943.e8. doi: 10.1016/j.neuron.2019.04.011

Adaikkan, C., & Tsai, L. H. (2020). Gamma Entrainment: Impact on Neurocircuits, Glia, and Therapeutic Opportunities. *Trends in Neurosciences*, *43*, 24–41. doi: 10.1016/j.tins.2019.11.001

Baillet, S. (2013). Forward and Inverse Problems of MEG/EEG. In *Encyclopedia of Computational Neuroscience* (pp. 1–8). New York, NY: Springer New York. doi: 10.1007/978-1-4614-7320-6_529-1

Bastos, A. M., & Schoffelen, J. M. (2016). A tutorial review of functional connectivity analysis methods and their interpretational pitfalls. *Frontiers in Systems Neuroscience*, *9*, 175. doi: 10.3389/fnsys.2015.00175

Bauer, F., Cheadle, S. W., Parton, A., Müller, H. J., & Usher, M. (2009). Gamma flicker triggers attentional selection without awareness. *Proceedings of the National Academy of Sciences of the United States of America*, *106*, 1666–1671. doi: 10.1073/pnas.0810496106

Bauer, M., Akam, T., Joseph, S., Freeman, E., & Driver, J. (2012). Does visual flicker phase at gamma frequency modulate neural signal propagation and stimulus selection? *Journal of Vision*, *12*, 1–10. doi: 10.1167/12.4.5

Başar-Eroglu, C., Strüber, D., Schürmann, M., Stadler, M., & Başar, E. (1996). Gamma-band responses in the brain: A short review of psychophysiological correlates and functional significance. *International Journal of Psychophysiology*, *24*, 101–112. doi: 10.1016/S0167-8760(96)00051-7

Besl, P. J., & McKay, N. D. (1992). A Method for Registration of 3-D Shapes. In *Ieee transactions on pattern analysis and machine intelligence* (Vol. 14, pp. 239–256). doi: 10.1109/34.121791

Brainard, D. H. (1997). The Psychophysics Toolbox. *Spatial Vision*, *10*, 433–436. doi: 10.1163/156856897X00357

Bressler, S. L. (1990). The gamma wave: a cortical information carrier? *Trends in Neurosciences*, *13*, 161–162. doi: 10.1016/0166-2236(90)90039-D

Brosch, M., Budinger, E., & Scheich, H. (2002). Stimulus-related gamma oscillations in primate auditory cortex. *Journal of Neurophysiology*, *87*, 2715–2725. doi: 10.1152/jn.2002.87.6.2715

Buffalo, E. A., Fries, P., Landman, R., Buschman, T. J., & Desimone, R. (2011). Laminar differences in gamma and alpha coherence in the ventral stream. *Proceedings of the National Academy of Sciences of the United States of America*, *108*, 11262–11267. doi: 10.1073/pnas.1011284108

Buzsáki, G., Horváth, Z., Urioste, R., Hetke, J., & Wise, K. (1992). High-frequency network oscillation in the hippocampus. *Science*, *256*, 1025–1027. doi: 10.1126/science.1589772

Buzsáki, G., & Wang, X. J. (2012). Mechanisms of gamma oscillations. *Annual Review of Neuroscience*, *35*, 203–225. doi: 10.1146/annurev-neuro-062111-150444

Carandini, M., Heeger, D. J., & Movshon, J. A. (1997). Linearity and normalization in simple cells of the macaque primary visual cortex. *Journal of Neuroscience*, *17*, 8621–8644. doi: 10.1523/jneurosci.17-21 -08621.1997

Colgin, L. L., Denninger, T., Fyhn, M., Hafting, T., Bonnevie, T., Jensen, O., ... Moser, E. I. (2009). Frequency of gamma oscillations routes flow of information in the hippocampus. *Nature*, *462*, 353–357. doi: 10.1038/nature08573

Connelly, W. M., Laing, M., Errington, A. C., & Crunelli, V. (2015). The thalamus as a low pass filter: Filtering at the cellular level does not equate with filtering at the network level. *Frontiers in Neural Circuits*, *9*, 89. doi: 10.3389/fncir.2015.00089

Cormack, L. K. (2005). Computational Models of Early Human Vision. In *Handbook of image and video processing* (pp. 325–345). Elsevier. doi: 10.1016/B978-012119792-6/50083-8

Dougherty, K., Cox, M. A., Ninomiya, T., Leopold, D. A., & Maier, A. (2017). Ongoing alpha activity in V1 regulates visually driven spiking responses. *Cerebral Cortex*, *27*, 1113–1124. doi: 10.1093/cercor/ bhv304

Douglas, R. J., & Martin, K. A. (2004). Neuronal circuits of the neocortex. *Annual Review of Neuroscience*, *27*, 419–451. doi: 10.1146/annurev.neuro.27.070203.144152

Drijvers, L., Spaak, E., & Jensen, O. (2020). Rapid invisible frequency tagging reveals nonlinear integration of auditory and visual semantic information. *bioRxiv*. doi: 10.1101/2020.04.29.067454

Eckhorn, R., Bauer, R., Jordan, W., Brosch, M., Kruse, W., Munk, M., & Reitboeck, H. J. (1988). Coherent oscillations: A mechanism of feature linking in the visual cortex? - Multiple electrode and correlation analyses in the cat. *Biological Cybernetics*, *60*, 121–130. doi: 10.1007/BF00202899

Engel, A. K., Fries, P., & Singer, W. (2001). Dynamic predictions: Oscillations and synchrony in top–down processing. *Nature Reviews Neuroscience*, *2*, 704–716. doi: 10.1038/35094565

Engel, A. K., Konig, P., & Singer, W. (1992). Synchronization of oscillatory neuronal responses in cat striate cortex: Temporal properties. *Visual Neuroscience*, *8*, 337–347. doi: 10.1017/S0952523800005071

Fiene, M., Schwab, B. C., Misselhorn, J., Herrmann, C. S., Schneider, T. R., & Engel, A. K. (2020). Phase-specific manipulation of rhythmic brain activity by transcranial alternating current stimulation. *Brain Stimulation*, *13*, 1254–1262. doi: 10.1016/j.brs.2020.06.008

Fries, P., Nikolić, D., & Singer, W. (2007). The gamma cycle. *Trends in Neurosciences*, *30*, 309–316. doi: 10.1016/j.tins.2007.05.005

Fröhlich, F. (2016). *Network Neuroscience*. Academic Press. doi: 10.1515/9781400851935-012

Gray, C. M., & Singer, W. (1989). Stimulus-specific neuronal oscillations in orientation columns of cat visual cortex. *Proceedings of the National Academy of Sciences of the United States of America*, *86*, 1698–1702. doi: 10.1073/pnas.86.5.1698

Grützner, C., Wibral, M., Sun, L., Rivolta, D., Singer, W., Maurer, K., & Uhlhaas, P. (2013). Deficits in high-($> 60$ hz) gamma-band oscillations during visual processing in schizophrenia. *Frontiers in Human Neuroscience*, *7*, 88. doi: 10.3389/fnhum.2013.00088

Gulbinaite, R., Roozendaal, D. H., & VanRullen, R. (2019). Attention differentially modulates the amplitude of resonance frequencies in the visual cortex. *NeuroImage*, *203*, 116–146. doi: 10.1016/j.neuroimage

630    .2019.116146

631    Haegens, S., Barczak, A., Musacchia, G., Lipton, M. L., Mehta, A. D., Lakatos, P., & Schroeder, C. E.

632      (2015). Laminar profile and physiology of the $\alpha$ rhythm in primary visual, auditory, and somatosensory

633      regions of neocortex. *Journal of Neuroscience*, *35*, 14341–14352. doi: 10.1523/JNEUROSCI.0600-15

634      .2015

635    Hanslmayr, S., Matuschek, J., & Fellner, M. C. (2014). Entrainment of prefrontal beta oscillations induces

636      an endogenous echo and impairs memory formation. *Current Biology*, *24*, 904–909. doi: 10.1016/

637      j.cub.2014.03.007

638    Hawken, M. J., Shapley, R. M., & Grosof, D. H. (1996). Temporal-frequency selectivity in monkey visual

639      cortex. , *13*, 477–492. doi: 10.1017/s0952523800008154

640    Helfrich, R. F., Breska, A., & Knight, R. T. (2019). Neural entrainment and network resonance in support

641      of top-down guided attention. *Current Opinion in Psychology*, *29*, 82–89. doi: 10.1016/j.copsyc.2018.12

642      .016

643    Hermes, D., Miller, K., Wandell, B., & Winawer, J. (2015). Stimulus dependence of gamma oscillations in

644      human visual cortex. *Cerebral Cortex*, *25*, 2951–2959. doi: 10.1093/cercor/bhu091

645    Herrmann, C. S. (2001). Human EEG responses to 1-100 Hz flicker: Resonance phenomena in visual cortex

646      and their potential correlation to cognitive phenomena. *Experimental Brain Research*, *137*, 346–353. doi:

647      10.1007/s002210100682

648    Herrmann, C. S., & Demiralp, T. (2005). Human EEG gamma oscillations in neuropsychiatric disorders.

649      *Clinical Neurophysiology*, *116*, 2719–2733. doi: 10.1016/j.clinph.2005.07.007

650    Herrmann, C. S., & Mecklinger, A. (2001). Gamma activity in human EEG is related to highspeed

651      memory comparisons during object selective attention. *Visual Cognition*, *8*, 593–608. doi: 10.1080/

652      13506280143000142

653    Hodge, R. D., Bakken, T. E., Miller, J. A., Smith, K. A., Barkan, E. R., Graybuck, L. T., . . . Others (2019).

654      Conserved cell types with divergent features in human versus mouse cortex. *Nature*, *573*, 61–68. doi:

655    10.1038/s41586-019-1506-7

656    Hoogenboom, N., Schoffelen, J. M., Oostenveld, R., & Fries, P. (2010). Visually induced gamma-band

657       activity predicts speed of change detection in humans. *NeuroImage*, *51*, 1162–1167. doi: 10.1016/

658       j.neuroimage.2010.03.041

659    Hoogenboom, N., Schoffelen, J. M., Oostenveld, R., Parkes, L. M., & Fries, P. (2006). Localizing human

660       visual gamma-band activity in frequency, time and space. *NeuroImage*, *29*, 764–773. doi: 10.1016/

661       j.neuroimage.2005.08.043

662    Hutcheon, B., & Yarom, Y. (2000). Resonance, oscillation and the intrinsic frequency preferences of

663       neurons. *Trends in Neurosciences*, *23*, 216–222. doi: 10.1016/S0166-2236(00)01547-2

664    Hutt, A., Griffiths, J. D., Herrmann, C. S., & Lefebvre, J. (2018). Effect of stimulation waveform on the

665       non-linear entrainment of cortical alpha oscillations. *Frontiers in Neuroscience*, *12*, 376. doi: 10.3389/

666       fnins.2018.00376

667    Iaccarino, H. F., Singer, A. C., Martorell, A. J., Rudenko, A., Gao, F., Gillingham, T. Z., … Tsai, L. H.

668       (2016). Gamma frequency entrainment attenuates amyloid load and modifies microglia. *Nature*, *540*,

669       230–235. doi: 10.1038/nature20587

670    Jensen, O., Kaiser, J., & Lachaux, J. P. (2007). Human gamma-frequency oscillations associated with

671       attention and memory. *Trends in Neurosciences*, *30*, 317–324. doi: 10.1016/j.tins.2007.05.001

672    Johns, P. (2014). *Clinical Neuroscience*. Elsevier Health Sciences. doi: 10.1016/c2009-0-35511-7

673    Kuffler, S. W. (1953). Discharge patterns and functional organization of mammalian retina. *Journal of*

674       *neurophysiology*, *16*, 37–68. doi: 10.1152/jn.1953.16.1.37

675    Kumpulainen, P. (n.d.). *Pekka Kumpulainen (2020). tight_subplot(Nh, Nw, gap, marg_-*

676       *h, marg_w) (https://www.mathworks.com/matlabcentral/fileexchange/27991-tight_subplot-nh-nw-gap-*

677       *marg_h-marg_w), MATLAB Central File Exchange.*

678    Lacadie, C. M., Fulbright, R. K., Arora, J., Constable, R. T., & Papademetris, X. (2007). Brodmann Areas

679       defined in MNI space using new Tracing Tool in BioImage Suite. In *Proceedings of the 14th annual*

680  *meeting of the organization for human brain mapping* (Vol. 36, p. 6494).

681  Lacadie, C. M., Fulbright, R. K., Rajeevan, N., Constable, R. T., & Papademetris, X. (2008). More accurate

682  Talairach coordinates for neuroimaging using non-linear registration. *NeuroImage*, *42*, 717–725. doi:

683  10.1016/j.neuroimage.2008.04.240

684  Lachaux, J. P., Rodriguez, E., Martinerie, J., & Varela, F. J. (1999). Measuring phase synchrony in

685  brain signals. *Human Brain Mapping*, *8*, 194–208. doi: 10.1002/(SICI)1097-0193(1999)8:4<194::

686  AID-HBM4>3.0.CO;2-C

687  Lee, S., & Jones, S. R. (2013). Distinguishing mechanisms of gamma frequency oscillations in human

688  current source signals using a computational model of a laminar neocortical network. *Frontiers in Human*

689  *Neuroscience*, *7*, 869. doi: 10.3389/fnhum.2013.00869

690  Müller, M. M., Junghöfer, M., Elbert, T., & Rochstroh, B. (1997). Visually induced gamma-band responses

691  to coherent and incoherent motion: A replication study. *NeuroReport*, *8*, 2575–2579. doi: 10.1097/

692  00001756-199707280-00031

693  Muthukumaraswamy, S. D., & Singh, K. D. (2013). Visual gamma oscillations: The effects of stimulus

694  type, visual field coverage and stimulus motion on MEG and EEG recordings. *NeuroImage*, *69*, 223–230.

695  doi: 10.1016/j.neuroimage.2012.12.038

696  Muthukumaraswamy, S. D., Singh, K. D., Swettenham, J. B., & Jones, D. K. (2010). Visual gamma

697  oscillations and evoked responses: Variability, repeatability and structural MRI correlates. *NeuroImage*,

698  *49*, 3349–3357. doi: 10.1016/j.neuroimage.2009.11.045

699  Nikolić, D., Fries, P., & Singer, W. (2013). Gamma oscillations: Precise temporal coordination without a

700  metronome. *Trends in Cognitive Sciences*, *17*, 54–55. doi: 10.1016/j.tics.2012.12.003

701  Nolte, G. (2003). The magnetic lead field theorem in the quasi-static approximation and its use for magne-

702  toenchephalography forward calculation in realistic volume conductors. *Physics in Medicine and Biology*,

703  *48*, 3637–3652. doi: 10.1088/0031-9155/48/22/002

704 Notbohm, A., Kurths, J., & Herrmann, C. S. (2016). Modification of brain oscillations via rhythmic light
705   stimulation provides evidence for entrainment but not for superposition of event-related responses. *Fron-*
706   *tiers in Human Neuroscience*, *10*, 10. doi: 10.3389/fnhum.2016.00010

707 Oostenveld, R., Fries, P., Maris, E., & Schoffelen, J. M. (2011). FieldTrip: Open source software for
708   advanced analysis of MEG, EEG, and invasive electrophysiological data. *Computational Intelligence and*
709   *Neuroscience*, *2011*, 115678–156869. doi: 10.1155/2011/156869

710 Orekhova, E. V., Butorina, A. V., Sysoeva, O. V., Prokofyev, A. O., Nikolaeva, A. Y., & Stroganova, T. A.
711   (2015). Frequency of gamma oscillations in humans is modulated by velocity of visual motion. *Journal*
712   *of Neurophysiology*, *114*, 244–255. doi: 10.1152/jn.00232.2015

713 Perry, G., Hamandi, K., Brindley, L. M., Muthukumaraswamy, S. D., & Singh, K. D. (2013). The properties
714   of induced gamma oscillations in human visual cortex show individual variability in their dependence on
715   stimulus size. *NeuroImage*, *68*, 83–92. doi: 10.1016/j.neuroimage.2012.11.043

716 Pikovsky, A., Kurths, J., Rosenblum, M., & Kurths, J. (2003). *Synchronization: a universal concept in*
717   *nonlinear sciences* (Vol. 12). USA: Cambridge University Press.

718 Ray, S., & Maunsell, J. H. (2011). Different origins of gamma rhythm and high-gamma activity in macaque
719   visual cortex. *PLoS Biology*, *9*. doi: 10.1371/journal.pbio.1000610

720 Ringach, D. L. (2004). Mapping receptive fields in primary visual cortex. *Journal of Physiology*, *558*,
721   717–728. doi: 10.1113/jphysiol.2004.065771

722 Roberts, M. J., Lowet, E., Brunet, N. M., TerWal, M., Tiesinga, P., Fries, P., & DeWeerd, P. (2013). Robust
723   gamma coherence between macaque V1 and V2 by dynamic frequency matching. *Neuron*, *78*, 523–536.
724   doi: 10.1016/j.neuron.2013.03.003

725 Rodriguez, E., George, N., Lachaux, J. P., Martinerie, J., Renault, B., & Varela, F. J. (1999). Perception's
726   shadow: Long-distance synchronization of human brain activity. *Nature*, *397*, 430–433. doi: 10.1038/
727   17120

728 Rolls, E. T., Huang, C. C., Lin, C. P., Feng, J., & Joliot, M. (2020). Automated anatomical labelling atlas 3.

729 *NeuroImage*, *206*, 116189. doi: 10.1016/j.neuroimage.2019.116189

730 Schadow, J., Lenz, D., Thaerig, S., Busch, N. A., Fründ, I., Rieger, J. W., & Herrmann, C. S. (2007). Stim-

731 ulus intensity affects early sensory processing: Visual contrast modulates evoked gamma-band activity

732 in human EEG. *International Journal of Psychophysiology*, *66*, 28–36. doi: 10.1016/j.ijpsycho.2007.05

733 .010

734 Schwab, K., Ligges, C., Jungmann, T., Hilgenfeld, B., Haueisen, J., & Witte, H. (2006). Alpha entrainment

735 in human electroencephalogram and magnetoencephalogram recordings. *NeuroReport*, *17*, 1829–1833.

736 doi: 10.1097/01.wnr.0000246326.89308.ec

737 Sharpee, T. O., Sugihara, H., Kurgansky, A. V., Rebrik, S. P., Stryker, M. P., & Miller, K. D. (2006).

738 Adaptive filtering enhances information transmission in visual cortex. *Nature*, *439*, 936–942. doi: 10

739 .1038/nature04519

740 Singer, W. (1999). Neuronal synchrony: A versatile code for the definition of relations? *Neuron*, *24*, 49–65.

741 doi: 10.1016/S0896-6273(00)80821-1

742 Singer, W. (2009). Distributed processing and temporal codes in neuronal networks. *Cognitive Neurody-

743 namics*, *3*, 189–196. doi: 10.1007/s11571-009-9087-z

744 Singer, W., & Gray, C. M. (1995). Visual feature integration and the temporal correlation hypothesis. *Annual

745 Review of Neuroscience*, *18*, 555–586. doi: 10.1146/annurev.ne.18.030195.003011

746 Spaak, E., Bonnefond, M., Maier, A., Leopold, D. A., & Jensen, O. (2012). Layer-specific entrainment of

747 gamma-band neural activity by the alpha rhythm in monkey visual cortex. *Current Biology*, *22*, 2313–

748 2318. doi: 10.1016/j.cub.2012.10.020

749 Spaak, E., de Lange, F. P., & Jensen, O. (2014). Local entrainment of alpha oscillations by vi-

750 sual stimuli causes cyclic modulation of perception. *Journal of Neuroscience*, *34*, 3536–3544. doi:

751 10.1523/JNEUROSCI.4385-13.2014

Stenroos, M., Hunold, A., Eichardt, R., & Haueisen, J. (2012). Comparison of three- and single-shell volume conductor models in magnetoencephalography. *Biomedizinische Technik*, *57*, 311. doi: 10.1515/bmt-2012-4396

Tallon, C., Bertrand, O., Bouchet, P., & Pernier, J. (1995). Gamma-range Activity Evoked by Coherent Visual Stimuli in Humans. *European Journal of Neuroscience*, *7*, 1285–1291. doi: 10.1111/j.1460-9568.1995.tb01118.x

Tallon-Baudry, C. (2009). The roles of gamma-band oscillatory synchrony in human visual cognition. *Frontiers in Bioscience*, *14*, 321–332. doi: 10.2741/3246

Tan, H. R., Gross, J., & Uhlhaas, P. J. (2016). MEG sensor and source measures of visually induced gamma-band oscillations are highly reliable. *NeuroImage*, *137*, 34–44. doi: 10.1016/j.neuroimage.2016.05.006

Tass, P., Rosenblum, M. G., Weule, J., Kurths, J., Pikovsky, A., Volkmann, J., . . . Freund, H. J. (1998). Detection of n:m phase locking from noisy data: Application to magnetoencephalography. , *81*, 3291–3294. doi: 10.1103/PhysRevLett.81.3291

Traub, R. D., & Whittington, M. (2010). *Cortical Oscillations in Health and Disease*. USA: Oxford University Press. doi: 10.1093/acprof:oso/9780195342796.001.0001

Traub, R. D., Whittington, M. A., Stanford, I. M., & Jefferys, J. G. (1996). A mechanism for generation of long-range synchronous fast oscillations in the cortex. *Nature*, *383*, 621–624. doi: 10.1038/383621a0

Uhlhaas, P. J., Pipa, G., Lima, B., Melloni, L., Neuenschwander, S., Nikolić, D., & Singer, W. (2009). Neural synchrony in cortical networks: History, concept and current status. *Frontiers in Integrative Neuroscience*, *3*, 17. doi: 10.3389/neuro.07.017.2009

Uhlhaas, P. J., & Singer, W. (2006). Neural synchrony in brain disorders: relevance for cognitive dysfunctions and pathophysiology. *Neuron*, *52*(1), 155–168.

Van Pelt, S., & Fries, P. (2013). Visual stimulus eccentricity affects human gamma peak frequency. *NeuroImage*, *78*, 439–447. doi: 10.1016/j.neuroimage.2013.04.040

41

776 Varela, F., Lachaux, J. P., Rodriguez, E., & Martinerie, J. (2001). The brainweb: Phase synchronization and

777 large-scale integration. *Nature Reviews Neuroscience*, *2*, 229–239. doi: 10.1038/35067550

778 Veen, B., Joseph, J., & Hecox, K. (1992). Localization of intra-cerebral sources of electrical activity

779 via linearly constrained minimum variance spatial filtering. *1992 IEEE 6th SP Workshop on Statistical*

780 *Signal and Array Processing, SSAP 1992 - Conference Proceedings*, *44*, 526–529. doi: 10.1109/SSAP

781 .1992.246899

782 Von der Malsburg, C. (1999). The what and why of binding: the modeler's perspective. *Neuron*, *24*,

783 95–104.

784 Wehr, M., & Laurent, G. (1996). Odour encoding by temporal sequences of firing in oscillating neural

785 assemblies. *Nature*, *384*, 162–166. doi: 10.1038/384162a0

786 Williams, P. E., Mechler, F., Gordon, J., Shapley, R., & Hawken, M. J. (2004). Erratum: Entrainment to

787 video displays in primary visual cortex of macaque and humans. *Journal of Neuroscience*, *24*, 8278–

788 8288.

789 Womelsdorf, T., Fries, P., Mitra, P. P., & Desimone, R. (2006). Gamma-band synchronization in visual

790 cortex predicts speed of change detection. *Nature*, *439*, 733–736. doi: 10.1038/nature04258

791 Xing, D., Yeh, C. I., Burns, S., & Shapley, R. M. (2012). Laminar analysis of visually evoked activity in the

792 primary visual cortex. *Proceedings of the National Academy of Sciences of the United States of America*,

793 *109*, 13871–13876. doi: 10.1073/pnas.1201478109

794 Zaehle, T., Rach, S., & Herrmann, C. S. (2010). Transcranial Alternating Current Stimulation Enhances

795 Individual Alpha Activity in Human EEG. *PLoS ONE*, *5*, e13766. doi: 10.1371/journal.pone.0013766

796 Zhigalov, A., Herring, J. D., Herpers, J., Bergmann, T. O., & Jensen, O. (2019). Probing cortical excitability

797 using rapid frequency tagging. *NeuroImage*, *195*, 59–66. doi: 10.1016/j.neuroimage.2019.03.056